



This is a repository copy of *Polariton condensation in a microcavity using a highly-stable molecular dye*.

White Rose Research Online URL for this paper:

<https://eprints.whiterose.ac.uk/185384/>

Version: Supplemental Material

---

**Article:**

McGhee, K.E., Jayaprakash, R., Georgiou, K. et al. (2 more authors) (2022) Polariton condensation in a microcavity using a highly-stable molecular dye. *Journal of Materials Chemistry C*, 10 (11). pp. 4187-4195. ISSN 2050-7526

<https://doi.org/10.1039/d1tc05554b>

---

© 2022 The Royal Society of Chemistry. This is an author-produced version of a paper subsequently published in *Journal of Materials Chemistry C*. Uploaded in accordance with the publisher's self-archiving policy.

**Reuse**

Items deposited in White Rose Research Online are protected by copyright, with all rights reserved unless indicated otherwise. They may be downloaded and/or printed for private study, or other acts as permitted by national copyright laws. The publisher or other rights holders may allow further reproduction and re-use of the full text version. This is indicated by the licence information on the White Rose Research Online record for the item.

**Takedown**

If you consider content in White Rose Research Online to be in breach of UK law, please notify us by emailing [eprints@whiterose.ac.uk](mailto:eprints@whiterose.ac.uk) including the URL of the record and the reason for the withdrawal request.



[eprints@whiterose.ac.uk](mailto:eprints@whiterose.ac.uk)  
<https://eprints.whiterose.ac.uk/>

# **Polariton condensation in a microcavity using a highly-stable molecular dye**

Kirsty E. McGhee<sup>1</sup>, Rahul Jayaprakash<sup>1</sup>, Kyriacos Georgiou<sup>1,2</sup>,

Stephanie L. Burg<sup>1</sup> and David G. Lidzey<sup>1\*</sup>

1. Department of Physics and Astronomy, University of Sheffield, Hicks Building, Hounsfield Road, Sheffield, S3 7RH, United Kingdom
2. Department of Physics, University of Cyprus, P.O. Box 20537, Nicosia 1678, Cyprus

## **Contents:**

1. Film properties
2. Coupled oscillator fits
3. Threshold calculation parameters
4. Origins of blueshift
5. Raman spectroscopy

## 1. Film properties

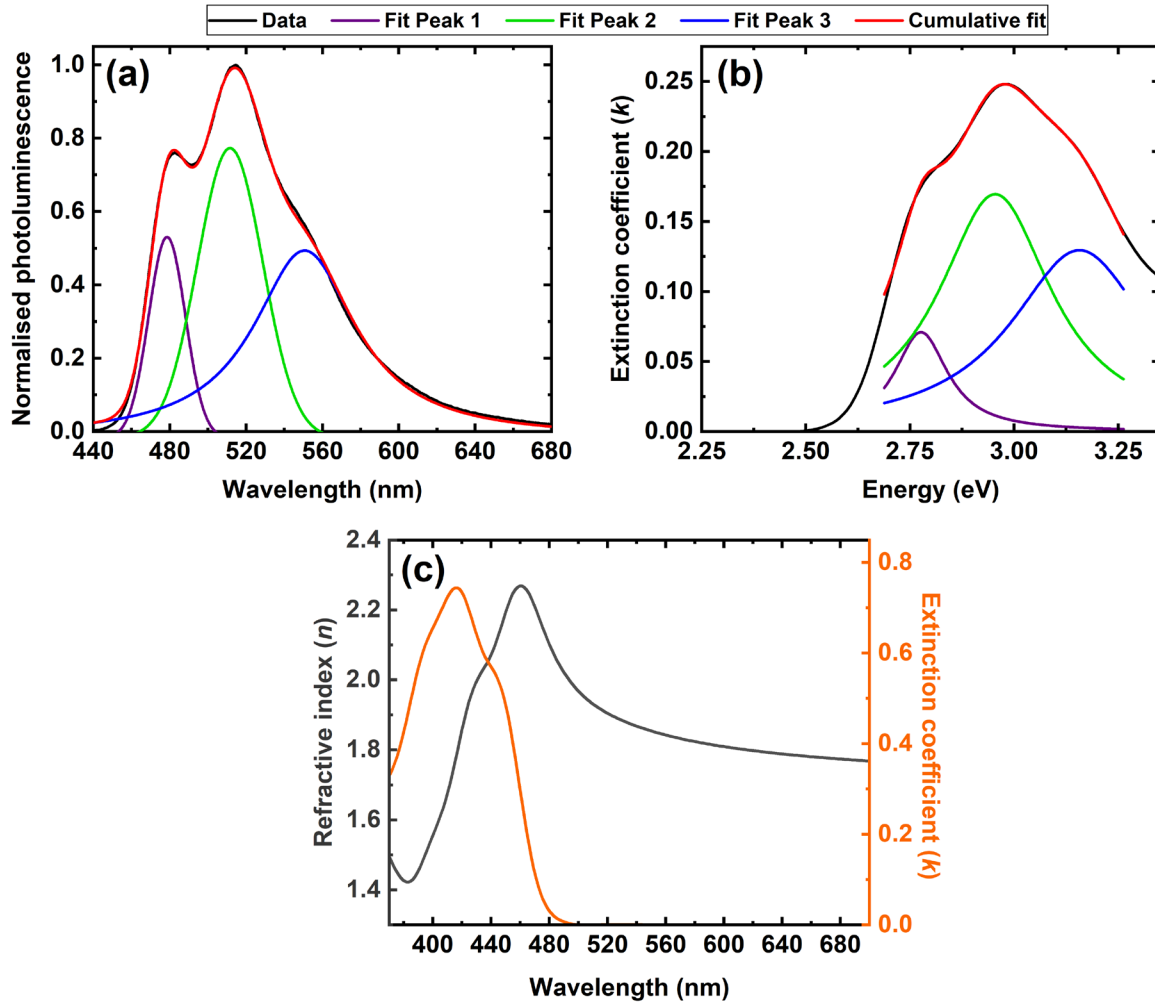


Figure S1. Multiple peak fits to DPAVB/PS film spectra and the ellipsometry data. Part (a) shows a triple-Voigt fit to the normalised photoluminescence, while part (b) shows a triple-Lorentzian fit to the calculated DPAVB/PS extinction coefficient. These Lorentzian functions are then used in the TMR model to describe the DPAVB transitions. Part (c) shows the refractive index and extinction coefficient obtained by ellipsometry for the pure DPAVB film.

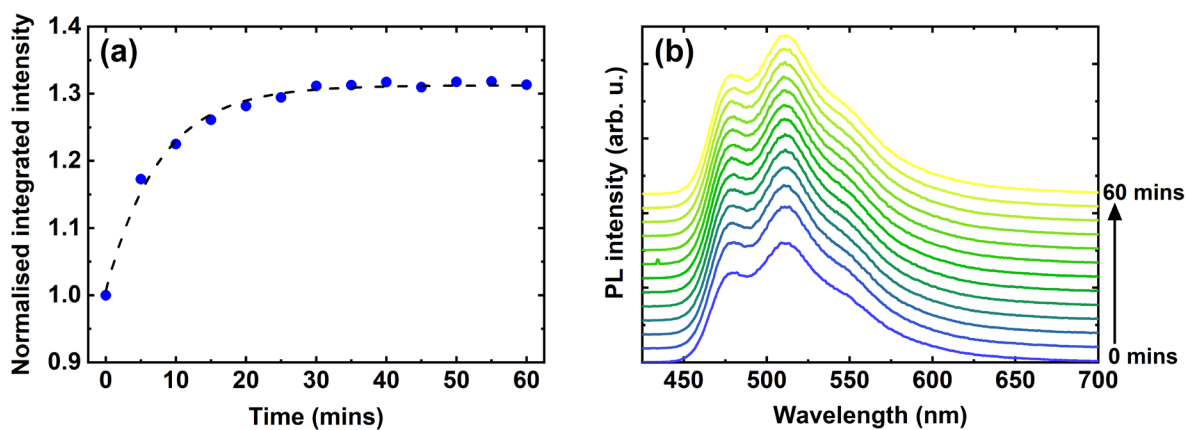


Figure S2. Photostability of DPAVB/PS film in the linear regime. Part (a) shows the time-dependence of the integrated PL intensity (blue circles) normalised to the value at time = 0 seconds. It can be seen that the PL intensity initially increases sharply and then saturates at ~130% of its initial value after about 30 minutes. The dashed line shows a single exponential fit to the data. Part (b) shows the PL spectra from 0 to 60 minutes at 5 minute intervals (with a constant  $y$ -offset), showing that while the intensity increases, its spectral shape remains the same.

## 2. Coupled oscillator fits

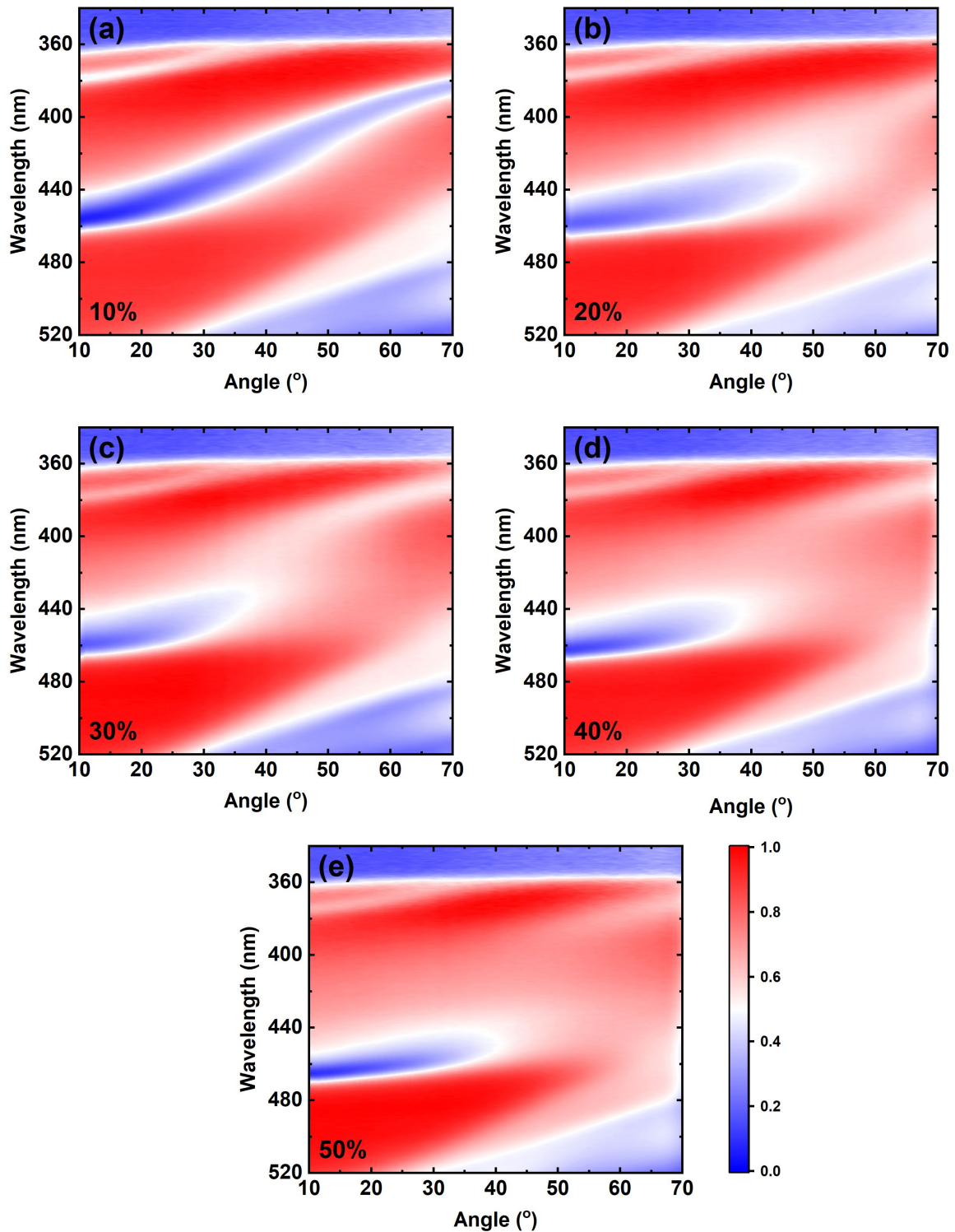


Figure S3. Angle-dependent white light reflectivity data for the DPAVB cavities with 6-pair DBRs. The DPAVB/PS concentration for each cavity was (a) 10%, (b) 20%, (c) 30%, (d) 40% and (e) 50%. It can be seen that at low concentrations the cavity is weakly-coupled, but that as the oscillator strength is increased, a splitting appears and the cavity enters the strong coupling regime.

Property	T1	T2	T3	Cavity mode
$\lambda_{peak}$ (nm)	447	420	393	483
$\gamma$ (meV)	78	164	203	3.4
$\Omega_{min}$ (meV)	110	232	287	/
$\Omega_{coupled}$ (meV)	168	260	227	/

Table S1. Parameters used to determine whether the various transitions within the 50% DPAVB/PS cavity with 6-pair DBRs are strongly-coupled. Here,  $\lambda_{peak}$  is the peak wavelength of each of the Lorentzian functions extracted from experimental data shown in Figure S1(b) and  $\gamma$  is their linewidth (half-width at half maximum). For the cavity mode,  $\lambda_{peak}$  and  $\gamma$  are the wavelength and half-width at half maximum at  $k = 0$  extracted from the TMR model. Using the condition described by Equation 1 (main paper), we indicate the minimum Rabi splitting,  $\Omega_{min}$ , at which the transitions should lie in the strong coupling regime.  $\Omega_{coupled}$  are the Rabi splittings deduced using the coupled oscillator model. From this it can be seen that T1 and T2 meet the condition (green text), whereas T3 does not (red text).

We have also fitted the higher Q-factor cavity based on 10 and 12-pair DBRs using a coupled oscillator model. The analysis of the cavity is complicated by that fact that no upper polariton branch is visible in either reflectivity measurements or in photoluminescence emission. We believe this is caused by a combination of large negative cavity detuning and the high reflectivity of the DBRs.

To fit the dispersion of the lower branch, we first determined whether the coupling constant ( $g$ ) changed when the DPAVB is placed in a 10/12 pair cavity compared to what is determined in a 6/6 pair cavity. Here we base our estimates on a similar system (BODIPY-Br in polystyrene) having a similar oscillator strength and an active layer of similar thickness. Using this, our TMR model indicates that the Rabi splitting is only expected to decrease by 2% when the number of DBR pairs is increased from 6/6 pairs to 10/12 pairs. Given the likely error associated with this estimate, we assume the Rabi splitting in the 10/12 cavity is the same as it is in the 6/6 cavity. We then use this as input to the coupled oscillator model (values of  $\Omega_1 = 168$  meV,  $\Omega_2 = 260$  meV and  $\Omega_3 = 227$  meV used in simulations) and fit to the measured reflectivity model as is shown below. Here, it can be seen that the fit to the LPB is very good; however, without a visible UPB, we treat this conclusion with a significant degree of caution.

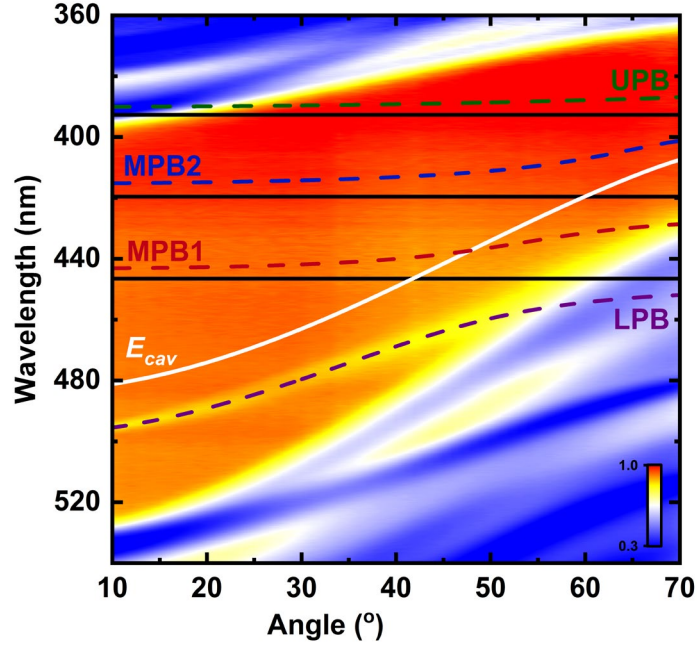


Figure S4. Coupled oscillator fit to 50% DPAVB cavity reflectivity with 10- and 12-pair DBRs. The fits to the LPB (purple), MPB1 (red), MPB2 (blue), and UPB (green) are shown by the dashed lines, while the cavity mode (white) and the DPAVB transitions (black) are shown by the solid lines. The labels for the transitions,  $T_1$ ,  $T_2$  and  $T_3$ , are not shown here for clarity, but they are the same as in Figures 2(c) and (d) of the main text.

### 3. Threshold calculation parameters

We detail our estimation of the threshold for amplified spontaneous emission (ASE) and polariton condensation below.

To calculate the ASE threshold, we first determined the relative absorption of a DPAVB/PS film at the excitation-laser wavelength. This was done by measuring the power of a 355 nm laser beam before (2.0  $\mu\text{W}$ ) and after (1.34  $\mu\text{W}$ ) transmission through a 200 nm thick DPAVB/PS film. We also measured the intensity of the reflected beam (0.17  $\mu\text{W}$ ). This indicates that 25% of incident laser power was absorbed by the film. This was then used with the laser repetition rate (100 Hz) and the excitation spot size (see Table S2), to convert the threshold power into a threshold fluence per pulse.

For the microcavity, we found that the intensity of incident laser is reduced by 40% as it passes through the bottom DBR (through which excitation is made). This suggests that the intensity of a 2.0  $\mu\text{W}$  laser beam (at 355 nm) would be reduced to 1.06  $\mu\text{W}$  as it passes into the active region. From the absorption coefficient of a 50% DPAVB/PS film (23,500  $\text{cm}^{-1}$ ) we estimate that a minimum of 28% of the incident laser is absorbed by the active layer (thickness = 317 nm). This simple calculation clearly neglects optical interference effects of the excitation laser-light within the cavity. This was again used with the laser repetition rate (100 Hz) and the excitation spot size (see Table S2), to convert the threshold power into a threshold fluence per pulse.

Parameters	ASE	Condensation
Power threshold ( $\mu\text{W}$ )	8.6	0.59
Spot size ( $\mu\text{m} \times \mu\text{m}$ )	6080 x 210	31.1 x 31.4
Spot area ( $\text{cm}^2$ )	$1.28 \times 10^{-2}$	$7.68 \times 10^{-6}$
% absorption at 355 nm	24.5	27.8
Fluence threshold ( $\mu\text{J}/\text{cm}^2$ )	1.7	215

Table S2. Parameters used for the calculation of the ASE and condensation thresholds.

#### 4. Origins of blueshift

To determine the origin of the blueshift, we performed two analyses and found the blueshift can be attributed to two mechanisms: a reversible photobleaching and an irreversible degradation of the DPAVB molecules in the cavity.

To demonstrate reversible photobleaching, we measured the emission from the LPB at a low power below threshold. We then measured the emission above threshold, and then below threshold again. Here emission was recorded using the same  $k$ -space setup used to obtain the data in Figures 3 and 4 of the main text. The spectra at  $k = 0$  are shown in Figure S5(a), where it can be seen that the emission blueshifts by 1.6 meV above threshold and then returns to its original position when excited below threshold. This clearly indicates that provided the cavity is not exposed for a prolonged period to a large laser flux, a substantial blueshift occurs that is fully reversible, and that this blueshift results from bleaching of the excitonic ground-state.

It is clear however that laser excitation does result in some degree of irreversible photodegradation – this is evidenced by the drop-off in intensity of polariton lasing as demonstrated in Figure 4(a) (Main paper). To assess the significance of this effect, we plotted the peak wavelength of the LPB emission above threshold (i.e. time-series data from Figure 4) as a function of number of pump pulses. This data is shown in Figure S5(b), where it can be seen that there is indeed a blueshift that occurs with increasing exposure. Here, we find that the LPB maximum undergoes a blueshift of 0.44 nm (2.2 meV) during the course of exposure to 37,750 laser pulses.

We have attempted to use the data in Fig S5(b) to explore the extent to which the power sweep data shown in Fig 3(b) (main paper) is determined by irreversible photodegradation. During the course of the power sweep measurements the sample received approximately 8,500 pulses (17 measurements, 5 s exposure, 100 Hz). However, the majority (82%) of the laser pulses during this measurement had a power lower than that used in the photostability measurement ( $2P_{th}$ ). At present, we do not understand how the photodegradation-rate scales with excitation-pump intensity, but suspect that any blue-shift due to photodegradation will be significantly less than that suggested by Figure 5(b) (0.55-1.1 meV at 8,500 pulses). We therefore conclude that the observed blueshift in Figure 3(b) can likely be attributed

to a combination of reversible photobleaching together with some irreversible photo-degradation, however the relative magnitude of these effects is at present unclear.

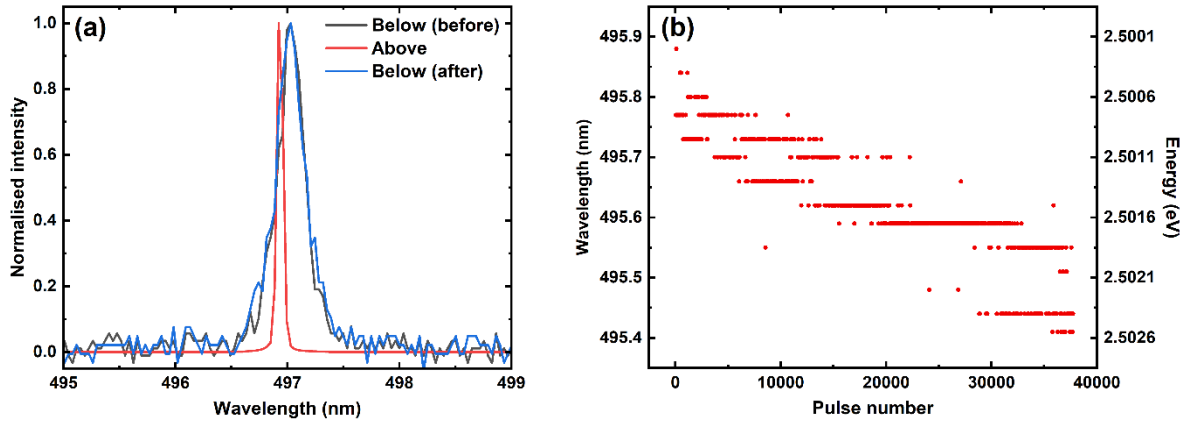


Figure S5. Origin of blueshift. Part (a) shows the normalised LPB spectra when the sample is first excited below threshold (before, grey), 1.7 times above threshold (red) and then again below threshold (after, blue). It can clearly be seen that the blueshift of the LPB above threshold is reversible. Part (b) shows the shift in emission wavelength of the condensate against pulse number at  $2P_{th}$ .

## 5. Raman spectroscopy

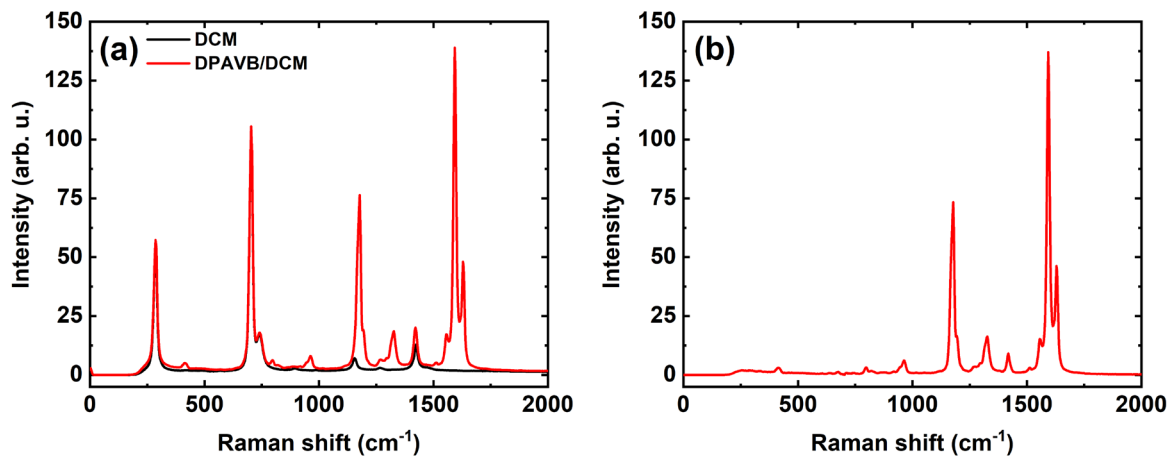


Figure S6. Raman spectra for DPAVB in dichloromethane (DCM). Part (a) shows the spectra for a pure DCM solution (black) and for a 10 mg/mL DPAVB/DCM solution (red). Part (b) shows the spectrum for pure DPAVB calculated by subtracting the two signals shown in part (a).